

Numerical Study of Reacting Flow in a Methane Burner with a Detailed Reaction Mechanism

Ayedh Alajmi^{a*}, Ibahim Abdalla^b, Jasem Alotaibi^c

^{a,c}*Public Authority for Applied Education and Training, Kuwait*

^b*Mechanical Engineering Department, De Montfort University, Leicester, UK*

^a*Email: ae.alajmi, jg.alotaibi@paeet.edu.kw*

^b*Email: iabdalla@dmu.ac.uk*

Abstract

In this paper, a numerical study of reacting flow in a methane burner using the Reynolds Averaged Navier-Stokes equation (RANS) is presented. A shear-stress transport turbulence model and presumed shape probability density functions (Pdfs) are used. Detailed chemical kinetic mechanism for the methane oxidation with 100 species and a 448 steps reaction has been developed using EXGAS software in this study. Moreover, simulations have been carried out to investigate the applicability of this study. The predicted temperature profiles agreed well with those obtained from Gas Research Institute (GRI) mechanism and the available experimental data. Other variables including CO₂ predicted by the GRI and the EXGAS mechanisms also show good agreement.

Keywords: Methane; EXGAS; GRI; Reaction mechanisms.

1. Introduction

The design of practical combustion devices such as industrial furnaces, gas turbines or internal combustion engines require an extensive knowledge of major chemical species, pollutants, and temperature. The characteristic features of these systems are complex geometries and even more complex chemical reaction mechanisms. Accurate and detailed numerical simulations of the combustion process in those devices require the solution of a large set of coupled differential equations, which require an impractically long time to solve with today's computers. One possible way to overcome this problem is to use the laminar flamelet concept [1].

* Corresponding author.

In laminar diffusion flamelets, scalar quantities (i.e., species' mass fractions, temperature and density) are unique functions of the mixture fraction and the scalar dissipation rate that can be pre-calculated and stored for further use. One important assumption used in this concept is that chemical reactions are relatively fast compared with the transport of chemical species and enthalpy driven by convective or diffusive forces [1]. The laminar flamelet concept introduces deviations from chemical equilibrium by means of the scalar dissipation rate [1], Poinso and Veynante [2], Champion and Libby [3], Launder and Spalding [4] and Liew and his colleagues [5]. The scalar dissipation rate can be interpreted as the reciprocal of a residence time for attaining chemical equilibrium. The laminar flamelet concept has also been applied to relatively slow chemical processes, i.e., the formation and destruction of soot in combustion systems (Balthasar and his colleagues [6], Pitsch and his colleagues [7], and Mauss and Balthasar [8]), as well as the oxidation of chlorinated hydrocarbons [9].

The application of the flamelet concept to model the formation of nitric oxides is open to debate. When modelling the formation of nitric oxides in turbulent diffusion flames, results from simulation conducted by Pfuderer and his colleagues [10] were lacking a consistent definition for the mixture fraction. Vranos and his colleagues [11] failed in modelling their turbulent methane-diffusion-flame satisfactorily with the stationary flamelet concept. Sanders and his colleagues [12] found a good agreement between flamelet-based simulations and experiments for the Nitrogen oxides (NO_x) concentration in the region of high Damköhler numbers. The flamelet calculations of Chen [13] show nitric oxide concentrations that surpass the experimentally determined values by about 200%. However, Chou and his colleagues [14] demonstrated that for a Bunsen-type flame a good agreement between measurements and simulations has been obtained using the flamelet concept.

In this paper, the steady-state laminar diffusion flamelet model is evaluated in the calculation of a methane diffusion flame. Moreover, a detailed reaction mechanism with 100 species and a 448 steps reaction for methane oxidation has been developed using EXGAS software [15]. Simulation has also been carried out using the kinetic mechanisms of the Gas Research Institute (GRI) including 49 species and a 279 steps reaction. The proposed model also takes into consideration thermal radiation using the P-1 radiation model. Soot formation and nitric oxide have not been taken into account. Moreover, in this paper, the predicted temperature is compared against those derived from the GRI mechanism and the experimental measurements.

2. Steady RANS Combustion Modeling

In this section, a brief description of the steady RANS combustion modelling is presented. Detailed mathematical formulation can be found in Poinso and Veynante [2], Champion and Libby [3], Williams [16], Borghi and Champion [17]. The equations governing flows with chemical reactions are related to continuity, the species conservation equations and energy. A solution to these equations provides, in principle, all the information required of a reacting flow. The equations for the mean quantities in the RANS approach are obtained by averaging the instantaneous governing equations using mass-weighted averages (Favre averages). This averaging procedure consists of splitting any instantaneous quantity f into a mean part - \tilde{f} and a fluctuating part - f'' :

$$f = \tilde{f} + f'' \quad \text{with} \quad \tilde{f}'' = 0 \tag{1}$$

The averaged governing equations can be written as follows:

- Mass:

$$\frac{\partial \bar{\rho}}{\partial t} + \frac{\partial}{\partial x_i}(\bar{\rho} \tilde{u}_i) = 0 \tag{2}$$

- Momentum:

$$\frac{\partial \bar{\rho} \tilde{u}_i}{\partial t} + \frac{\partial}{\partial x_i}(\bar{\rho} \tilde{u}_i \tilde{u}_j) + \frac{\partial \bar{p}}{\partial x_j} = \frac{\partial}{\partial x_i}(\bar{\tau}_{i,j} - \bar{\rho} \tilde{u}_i'' \tilde{u}_j'') \tag{3}$$

- Chemical Species

$$\frac{\partial(\bar{\rho} \tilde{Y}_k)}{\partial t} + \frac{\partial}{\partial x_i}(\bar{\rho} \tilde{u}_i \tilde{Y}_k) = -\frac{\partial}{\partial x_i}(\bar{V}_{k,i} \bar{Y}_k + \bar{\rho} \tilde{u}_i'' \tilde{Y}_k'') + \bar{\omega}_k \quad \text{For } k = 1, N \tag{4}$$

- Enthalpy

$$\frac{\partial \bar{\rho} \tilde{h}_s}{\partial t} + \frac{\partial}{\partial x_i}(\bar{\rho} \tilde{u}_i \tilde{h}_s) = \bar{\omega}_T + \frac{\overline{Dp}}{Dt} + \frac{\partial}{\partial x_i}(\lambda \frac{\partial \bar{T}}{\partial x_i} - \overline{\rho u_i'' h_s''}) + \tau_{i,j} \frac{\partial u_i}{\partial x_j} - \frac{\partial}{\partial x_i}(\overline{\rho \sum_{k=1}^N h_{s,k} Y_k V_{k,i}}) \tag{5}$$

Where

$$\frac{\overline{DP}}{Dt} = \frac{\partial \bar{p}}{\partial t} + u_i \frac{\partial \bar{p}}{\partial x_i} = \frac{\partial \bar{p}}{\partial t} + \tilde{u}_i \frac{\partial \bar{p}}{\partial t} + u'' \frac{\partial \bar{p}}{\partial x_i} \tag{6}$$

The averaging procedure introduces unclosed quantities which must be modelled.

- Species $((\tilde{u}_i'' \tilde{Y}_k''))$ and enthalpy $((\tilde{u}_i'' \tilde{h}_s''))$ turbulent fluxes:

The fluxes are generally closed using a classical gradient assumption:

$$\overline{\rho u_i'' \tilde{Y}_k''} = -\frac{\mu_t}{Sc_{kt}} \frac{\partial \tilde{Y}_k}{\partial x_i} \tag{7}$$

Where μ_t is the turbulent viscosity, estimated from the turbulence model, and Sc_{kt} a turbulent Schmidt number

for species k .

- Laminar diffusive fluxes for species or enthalpy:

These molecular terms are generally neglected against turbulent transport, assuming a sufficiently large turbulence level (large Reynolds number limit). They may also be retained by adding a laminar diffusivity to the turbulent viscosity μ_t in (7).

$$\overline{V_{k,i} Y_k} = -\overline{\rho D_k \frac{\partial Y_k}{\partial x_i}} \approx -\overline{\rho} \overline{D_k} \frac{\partial \tilde{Y}_k}{\partial x_i} \quad (8)$$

where \overline{D} is mean species molecular diffusion coefficient. The laminar heat diffusion flux in the enthalpy equation is generally written as:

$$\overline{\lambda \frac{\partial T}{\partial x_i}} = \overline{\lambda} \frac{\partial \tilde{T}}{\partial x_i} \quad (9)$$

Where $\overline{\lambda}$ is the mean thermal diffusivity.

- Pressure-velocity correlation $\overline{(u'_i \partial p / \partial x_i)}$:

This term allows only the determination of mean quantities that may be quite different from instantaneous quantities. It is not considered in this paper.

3. Turbulence Model

The Reynolds stresses term $(u'_i u'_j)$ is approximated by a turbulence model. In this paper, Shear-Stress Transport (SST) turbulence is employed which has a similar form to the Wilcox $k - \omega$ model. The SST model combines the advantages of the Wilcox $k - \omega$ and the $k - \epsilon$ model, using the standard $k - \omega$ model in the inner region of the boundary layer and a high-Reynolds-number version of the $k - \epsilon$ model in the outer region of the boundary layer.

$$\frac{\partial}{\partial t}(\overline{\rho k}) + \frac{\partial}{\partial x_i}(\overline{\rho u_i k}) = \frac{\partial}{\partial x_i}[(\mu + \frac{\mu_t}{\sigma_k}) \frac{\partial k}{\partial x_i}] + P_k - \beta' \overline{\rho k} \omega \quad (10)$$

$$\frac{\partial}{\partial t}(\overline{\rho \omega}) + \frac{\partial}{\partial x_i}(\overline{\rho u_i \omega}) = \frac{\partial}{\partial x_i}[(\mu + \frac{\mu_t}{\sigma_\omega}) \frac{\partial \omega}{\partial x_i}] + (1 - F_1) 2\overline{\rho} \frac{1}{\sigma_{\omega 2} \omega} \frac{\partial k}{\partial x_i} \frac{\partial \omega}{\partial x_i} + \alpha_2 \frac{\omega}{k} P_k - \beta_2 \overline{\rho} \omega^2 \quad (11)$$

The model constants are given by:

$$\beta' = 0.09, \sigma_k = 1.176, \sigma_\omega = 2, \alpha_2 = 0.44, \beta_2 = 0.0828, \sigma_{\omega 2} = 1.16$$

The equation of ω is multiplied by blending function $1 - F_1$ to ensure that the model equations behave

appropriately in both the near-wall and far-field zones.

The modified turbulent viscosity is calculated by:

$$\mu_t = \frac{a_1 k \bar{\rho}}{\max(a_1 \omega, S F_2)} \quad (12)$$

where F_2 is blending function similar to F_1 , which restricts the limiter to the wall boundary layer. S is the strain rate tensor and $a_1 = 0.31$.

The blending functions are critical to the success of the method. Their formulation is based on the distance to the nearest surface and on the flow variables.

$$F_1 = \tanh(\arg_1^4) \quad (13)$$

With

$$\arg_1 = \min\left(\max\left(\frac{\sqrt{k}}{\beta' \omega y}, \frac{500\nu}{y^2 \omega}\right), \frac{4\bar{\rho}k}{CD_{k\omega} \sigma_{\omega 2} y^2}\right) \quad (14)$$

Where y is the distance to the nearest wall ν is the kinematic viscosity. The cross-diffusion (CD) term is determined as:

$$CD_{k,\omega} = \max\left(2\bar{\rho} \frac{1}{\sigma_{\omega 2} \omega} \frac{\partial k}{\partial x_i} \frac{\partial \omega}{\partial x_i}, 1.0 \times 10^{-10}\right) \quad (15)$$

$$F_2 = \tanh(\arg_2^2) \quad (16)$$

With

$$\arg_2 = \max\left(\frac{2\sqrt{k}}{\beta' \omega y}, \frac{500\nu}{y^2 \omega}\right) \quad (17)$$

A disadvantage of the standard two-equation turbulence models is the excessive generation of turbulence energy, P_k in the vicinity of stagnation points. In order to avoid the build-up of turbulent kinetic energy in stagnation regions, a formulation of limiters for the production term in the turbulence equations is introduced by Menter [18].

$$P_k = \mu_t \frac{\partial \tilde{u}_i}{\partial x_j} \left(\frac{\partial \tilde{u}_i}{\partial x_j} + \frac{\partial \tilde{u}_j}{\partial x_i} \right) \rightarrow \tilde{P}_k = (P_k, 10\rho\beta k\omega) \quad (18)$$

4. Combustion Model

The chemical reaction source term in (4) will be calculated using the laminar flamelet model (LFM) (Peters [1]) and the turbulent flame is assumed to be comprised of an ensemble of small laminar flamelets. Although turbulence can influence the internal structure of the flamelets through flame straining and curvature, a laminar structure is retained.

Solution of the turbulent flame can therefore be achieved, given the characteristics of the laminar flamelets that represent the instantaneous reaction zones.

The laminar flamelet theory is described in detail in [1,2,3,4,5,19]. The LFM enables a very cost-effective and sequential investigation of thermo-chemical and hydrodynamic phenomena. Laminar flames, representing an instantaneous structure of the turbulent flame front, subjected to a certain state of disturbances by the turbulent motion, are computed a priori.

Information obtained by these computations is used as a database (flamelet library) for the subsequent computation of the multi-dimensional turbulent flame.

The flamelet data is characterized by a few key scalar parameters, the statistics of which are calculated in the turbulent flame computation. The incorporation of detailed chemistry is allowed, since it is applied within confines of a laminar system.

The extreme closure difficulties associated with bringing in full chemistry within a turbulent calculation do therefore not occur and the chemical mechanism used within the laminar flame does not lead to increased computational requirements within the turbulent flame computation.

The influence of turbulent fluctuations on the chemical system can be described with the help of probability density functions (PDFs). The mean value of a quantity tabulated in the flamelet library is derived from the following integration:

$$\bar{\Phi}(x, r) = \int_0^\infty \int_0^1 \Phi(\xi, \chi_{st}) PDF(\xi, \chi_{st}; x, r) d\xi d\chi_{st}. \quad (19)$$

For the assumption of statistical independence, $PDF(\xi, \chi_{st}; x, r)$ can be written as:

$$PDF(\xi, \chi) = PDF(\xi).PDF(\chi). \quad (20)$$

For the PDF of the mixture fraction, a β –function has been assumed:

$$PDF(\xi) = \frac{\xi^{\alpha-1}(1-\xi)^{\beta-1}}{\int_0^1 \xi^{\alpha-1}(1-\xi)^{\beta-1} d\xi} = \frac{\Gamma(\alpha+\beta)}{\Gamma(\alpha)\Gamma(\beta)} \xi^{\alpha-1}(1-\xi)^{\beta-1}. \quad (21)$$

Where $\Gamma(x)$ is:

$$\Gamma(x) = \int_0^{\infty} e^{-t} t^{x-1} dt. \quad (22)$$

The parameters α and β are functions of the mean value and the variance of the mixture fraction respectively.

$$\alpha = \frac{\tilde{\xi}^2(1 - \tilde{\xi})}{\tilde{\xi}''} - \tilde{\xi}, \quad \beta = \alpha \left(\frac{1 - \tilde{\xi}}{\tilde{\xi}} \right) \quad (23)$$

The PDF of the scalar dissipation rate PDF(χ_{st}) is assumed to have the shape of a logarithmic normal distribution:

$$PDF(\chi_{st}) = \frac{\log e}{\chi_{st} \sigma_{log} \sqrt{2\pi}} \text{Exp} \left(-\frac{(\log \chi_{st} - \mu_{log})^2}{2\sigma_{log}^2} \right). \quad (24)$$

The parameters μ_{log} and σ_{log} stand for the mean value and the variance of the transformed property $f_x = \log \chi_{st}$. They are derived from the mean value and the variance of the scalar dissipation rate as follows:

$$\chi_{st} = \text{Exp} \left(\mu_{log} + \frac{\sigma_{log}^2}{2} \right), \quad (25)$$

$$\chi_{st}''^2 = \text{Exp}(\sigma_{log}^2 - 1) \text{Exp}(2\mu_{log} + \sigma_{log}^2). \quad (26)$$

The equation of the mean value of the scalar dissipation rate χ_{st} is modelled as:

$$\chi_{st} = C_{\chi} \xi''^2 \frac{\tilde{\xi}}{k} \quad \text{with} \quad C_{\chi} = 2. \quad (27)$$

μ_{log} can be calculated from the above equations and σ_{log} is assumed to have a value of $\sigma_{log} = \sqrt{2}$. The work of Liew and his colleagues [20] shows only little influence of the exact value of σ_{log} on the results obtained from flamelet calculations.

4.1 Chemical mechanism

The chemical models used in this study are:

4.1.1 Gas Research Institute mechanism

The Gas Research Institute (GRI) mechanism, version 2.11 Bowman and his colleagues [21], is used in this paper. It consists of 49 chemical species and 279 reactions, describes the oxidation of methane, and contains a comprehensive set of reactions for the formation and reduction of Nitrogen monoxide (NO). Therefore, the

flamelet calculations for the laminar methane (CH₄)/air-diffusion flame presented below include the destruction of NO by convection into the fuel-rich side of the flame.

4.1.2 EXGAS mechanism

Detailed kinetic mechanism for the methane oxidation has been developed using the EXGAS computer package. This software has been used for generating mechanisms for the alkanes (Warth and his colleagues [22], Buda and his colleagues [23], Biet and his colleagues [24], Glaude and his colleagues [25] and Touchard and his colleagues [26]). The mechanism considered in this paper is based on 100 species and 448 steps reaction. A summary of both the mechanisms is given in Table 1.

Table 1: Chemical Reaction Mechanisms

Mechanism	GRI	EXGAS
Number of reactions	279	448
Number of species	49	100

5. Radiation Model

Including the radiation modelling offers the capability of slightly increased accuracy, but may cause flamelets to be extinguished at low strain rates. Hence, the radiation source term should be treated with caution [1]. The radiation model used in this paper is the P-1 model. It is the simplest case of the more general P-N model, which is based on the expansion of the radiation intensity I into an orthogonal series of spherical harmonics [27]. The following equation is used for the radiation flux q_r :

$$q_r = -\frac{1}{3(\alpha + \sigma_s) - C\sigma_s} \nabla G \quad (28)$$

Where α is the absorption coefficient, σ_s is the scattering coefficient, G is the incident radiation, and C is the linear anisotropic phase function coefficient. It ranges from -1 to +1 and represents the amount of radiation scattered in forward direction. A positive value indicates that more radiant energy is scattered forward than backward with $C = 1$ standing for complete backward scattering. A zero value of C defines isotropic scattering. This approximation is implemented in the results of the simulations presented in this paper.

The transport equation for G is:

$$\nabla \left(\frac{1}{3(\alpha + \sigma_s) - C\sigma_s} \nabla G \right) - \alpha G + 4\alpha\sigma T^4 = 0 \quad (29)$$

Where σ is the Stefan-Boltzmann constant. Combining (28) and (29), one obtains:

$$-\nabla q_r = \alpha G + 4\alpha\sigma T^4 = 0 \quad (30)$$

where the expression for radiation's flux gradient can be directly substituted into the energy equation to account for heat sources or sinks due to radiation. The flux of the radiation at walls, $q_{r,w}$, can be calculated from e_w , the wall emissivity.

$$q_{r,w} = -\frac{e_w}{2(2 - e_w)}(4\sigma T_w^4 - G_w) \quad (31)$$

5.1 Flame radiation losses

The determination of the Planck-mean absorption coefficient takes into account the effect of the gas band radiation. For gas band radiation, carbon dioxide (CO₂) and water (H₂O) are the most important radiating species in hydrocarbon flames. Carbon monoxide (CO) and methane (CH₄) contribute much less to the flame temperature reduction than do CO₂ and H₂O. However, considering all four species in a radiation model is suggested [28].

The Planck coefficients for CH₄, H₂O, (CO) and carbon dioxide (CO₂) were taken from the RADCAL program of Grosshandler [29]. The planck mean absorption coefficient for CO₂, H₂O, CH₄ and CO as function of gas temperature [29] is shown in the Fig. 1.

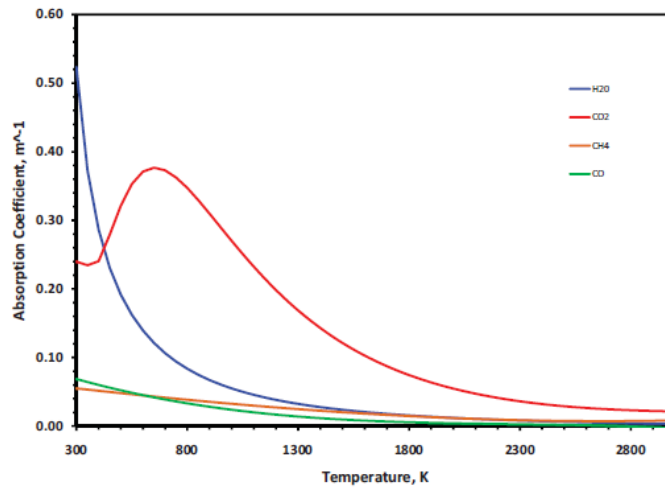


Figure 1: Planck mean absorption coefficient for CO₂, H₂O, CH₄ and CO as function of gas temperature [29]

6. Computational Procedure

The first step in defining the flamelet is to understand the species and reaction definitions for the chemical system. The species', thermodynamic, transport and reaction data must be in CHEMKIN format. The steady flamelet is generated and the integrated reaction rate Ω_k and Ω_T as function of the mean scalar dissipation rate from k and ε are stored. In the Computational Fluid Dynamics (CFD) code of Fluent, the flame surface density Σ is solved and finally the species' $\bar{\omega}_k$ mean reaction rates and the temperature $\bar{\omega}_k$ mean reaction rate are

computed.

6.1 Geometry

The combustor considered in this paper has a cylindrical shape with 0.6 m of diameter and total length of 2 m. The fuel inlet diameter is 0.01 m and the air inlet diameter is 0.3 m. The dimensions and other parameters such as fuel rate and relevant boundary conditions as well as the experimental data used are taken from the work of Ilbasa and his colleagues [30]. The physical domain of the combustor is given in Fig. 2.

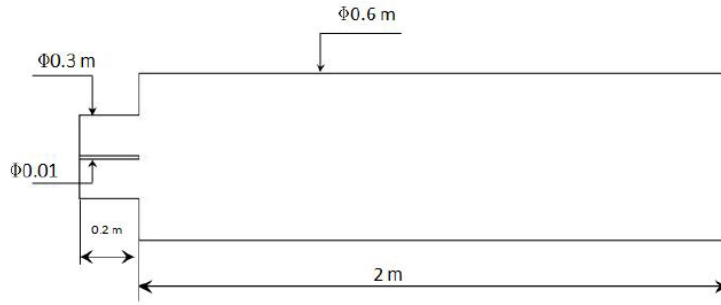


Figure 2: Geometry

6.2 Mesh generation

The goal is to determine the required near-wall mesh spacing, Δy in terms of Reynolds number, running length, and a Δy^+ target value. A hybrid method is developed by Menter [18] for the SST turbulence model (automatic near-wall treatment) which automatically switches from a low- Re formulation to wall functions based on the grid spacing. The SST has the advantage that an analytical expression is known for ω in the viscous sub-layer, which can be exploited to achieve this goal. The main idea behind the present formulation is to blend the wall value for ω between the logarithmic and the near-wall formulation. The flux for the k-equation is artificially kept to be zero and the flux in the momentum equation is computed from the velocity profile.

The equations are as follows. Flux for the momentum, F_U :

$$F_U = -\rho u_\tau u^* \quad (32)$$

With

$$u_\tau = \sqrt{\nu \left| \frac{\Delta U}{\Delta y} \right|_w} \quad (33)$$

And

$$u^* = \max(\sqrt{a_1 k}, u_\tau) \tag{34}$$

Flux for the k-equation:

$$F_k = 0 \tag{35}$$

In the ω -equation, an algebraic expression is specified instead of an added flux. It is blended between the analytical expression for ω in the logarithmic region:

$$\omega_l = \frac{u^*}{a_1 \kappa y} = \frac{1}{a_1 \kappa y} \frac{u^{*2}}{y^+} \tag{36}$$

where K is the Von Karmen constant. The corresponding expression in the sub layer:

$$\omega_s = \frac{6\nu}{\beta(\Delta y)^2} \tag{37}$$

with Δy being the distance between the first and the second mesh point. In order to achieve a smooth blending and avoid cyclic convergence behaviour, the following formulation is selected:

$$\omega_\omega = \omega_s \sqrt{1 + \left(\frac{\omega_l}{\omega_s}\right)^2} \tag{38}$$

This formulation provides the optimal boundary condition for a given grid. This strength of this method is that it allows for an accurate near-wall treatment over a wide range of grid spacing. It requires a minimum of at least 10 grid nodes inside the boundary layer. The estimates are based on the following correlations:

$$\Delta y = L \Delta y^+ \sqrt{80 Re_L^{-0.9285}} \tag{39}$$

where L is the computational domain length, Δy is the near-wall mesh size, Δy^+ is the target value. Setting the target to 1 for incoming velocity $V_\infty = 0.43\text{m/s}$ require a near-wall mesh space of $6.8 \times 10^{-4}\text{m}$.

Multi-bloc structured mesh has been generated which has the topology as shown in Fig. 3, with near-size wall given by (36).

The total grid points are 400,000. The resulting Y^+ near walls is between 1 - 1.3.

6.3 Determining turbulence parameters

Two parameters must be determined at the inlet flow: the turbulence intensity (I), and the turbulent length scale (l). The turbulence intensity can be estimated from the following formula derived from an empirical

correlation for pipe flows:

$$I \equiv \frac{u'}{u_{avg}} = 0.16(Re)^{-1/8} \tag{40}$$

$$l = C_{\mu} \frac{k^{3/2}}{\varepsilon} \tag{41}$$

The turbulence length scale ‘*l*’ is a physical quantity related to the size of the large eddies that contain the energy in turbulent flows. An approximation can be made using the following formula.

This correlation is not necessarily applicable to all situations; however, it is a valid approximation.

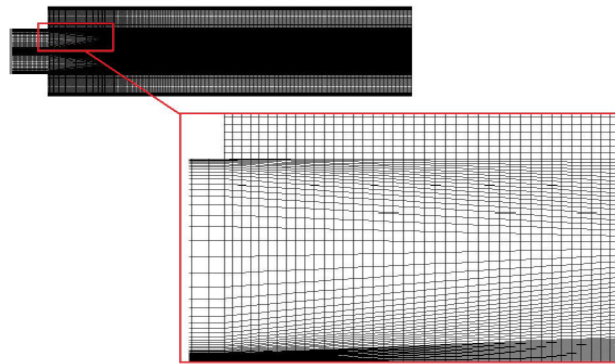


Figure 3: Mesh topology

6.4 Boundary conditions

6.4.1 Inflow conditions

All flow quantities at the boundary are prescribed. Table 2 presents the quantities required at the inlet and the fuel flow rate is $Q_f = 4.467 \times 10^{-4}$ kg/s.

Table 2: Turbulence Intensity and Turbulence Length Scale

V_{∞}	P	T	I	l
(m/s)	atm	K	(%)	(m)
0.34	1	300	4.73×10^{-2}	3.23×10^{-3}

6.4.2 Outflow condition

The zero gradient outflow boundary condition is used to model flow at the exit of the domain, where the details of the flow velocity and pressure are not known prior to solution of the flow problem.

6.4.3 Wall boundary

A no-slip boundary condition is applied on all the walls. In this paper, the combustor wall is treated as adiabatic and catalytic. Taking into account the radiation effect, the walls are treated as a grey heat sink of emissivity 1. The wall scattering coefficient is taken as zero.

7. Results and Discussion

Calculations of the diffusion flame were carried out at atmospheric pressure for the stoichiometric condition. A chemical reaction mechanism has been developed for the methane oxidation using EXGAS computer package, the mechanism is based on 100 species and 448 steps reaction.

The GRI and EXGAS mechanisms predict qualitatively similar temperature distribution at the flow exit of the domain ($x = 2$ m). The results from the simulation are also compared with the temperature measurements from Ibasa and his colleagues [30] experiment. Results of the EXGAS mechanism shows slightly better agreement with the experimental data than those obtained from the GRI mechanism. However, it is worth pointing that the temperature distribution is strongly de-pendent on the flow field and the current predicted flow field from the RANS approach may not be accurate enough. Therefore, it is highly likely that the discrepancy between the predictions and the experimental data is partly due to this reason.

The overall shapes of the temperature distribution obtained from both mechanisms are more or less identical with the maximum temperatures occurring at the same distance ($x \approx 1.2m$) in the centerline region as can be seen from this figure. However, there are some very small differences in the predicted temperature fields in certain regions.

The Maximum predicted temperature from EXGAS is $T_{max} = 1957K$ while $T_{max} = 1971K$ is predicted from the GRI mechanism. This indicates that the GRI and the EXGAS mechanisms show almost negligible difference in terms of temperature predictions.

The predicted distributions of mass fractions of two major species H_2O and CO_2 along the centerline are shown in Fig. 4 and Fig. 5 respectively.

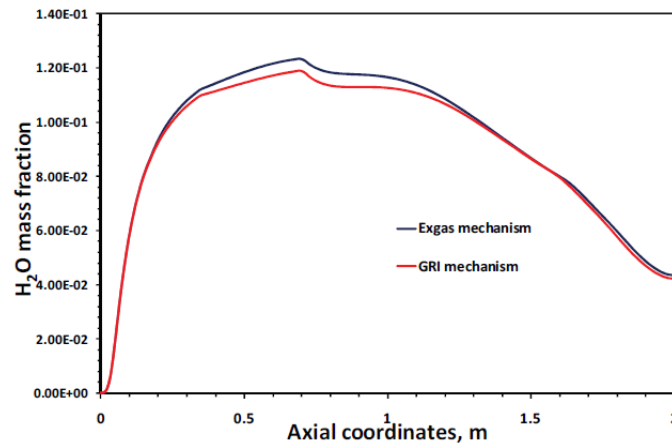


Figure 4: Comparison of the CFD predicted H₂O at the center line

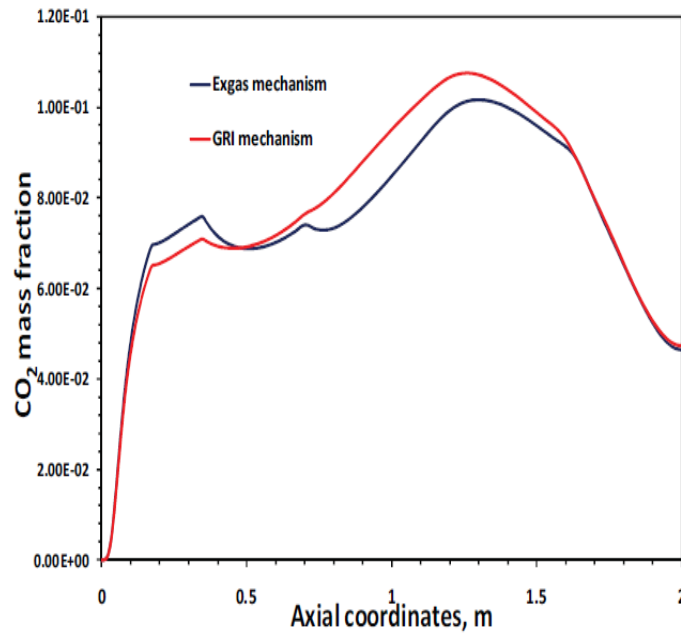


Figure 5: Comparison of the CFD predicted CO₂ at the center line.

The profiles predicted from both mechanisms are very similar. The predicted peaks of mass fraction of H₂O are located in the same region in the flame ($x = 0.7$ m) with a slightly high concentration of 3.4% predicted from the EXGAS mechanism.

The mass fraction of CO₂ predicted from the GRI mechanism is higher than that from the EXGAS mechanism in most of the region along the centreline, with the maximum difference of around 6%. The mass fraction contours of H₂O and CO₂ are presented in Fig. 6 and Fig. 7 over the whole domain.

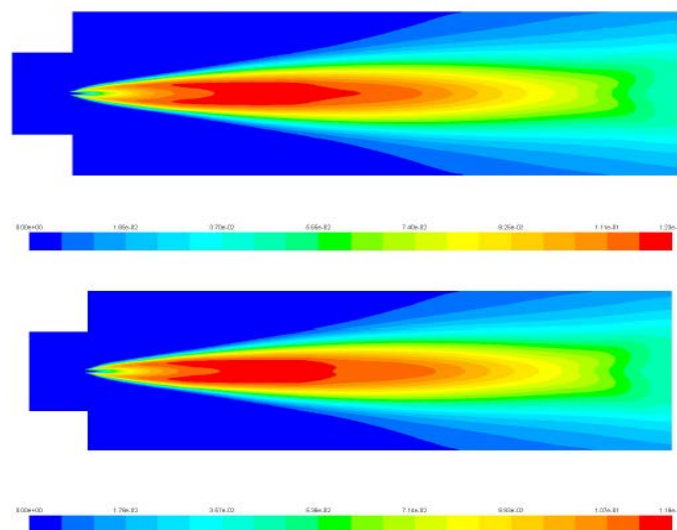


Figure 6: H₂O contours, EXGAS mechanism (top), GRI mechanism (bottom)

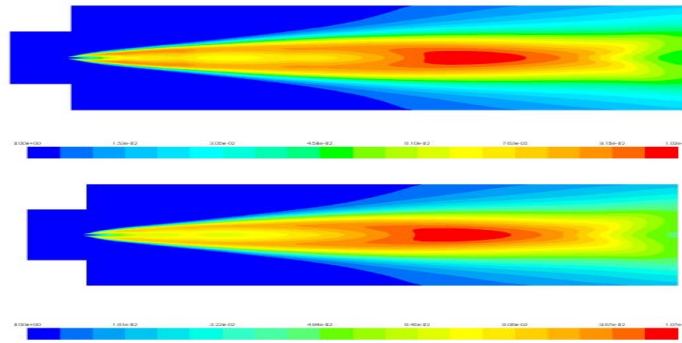


Figure 7: CO₂ contours, EXGAS mechanism (top), GRI mechanism (bottom)

Similar to the profiles along the centreline, it can be seen that the results from the EXGAS mechanism correlate quite well with those derived from the GRI mechanism.

However, the trends change when looking at the predicted distribution of the CO mass fraction from both mechanisms as shown Fig. 8 and Fig. 9.

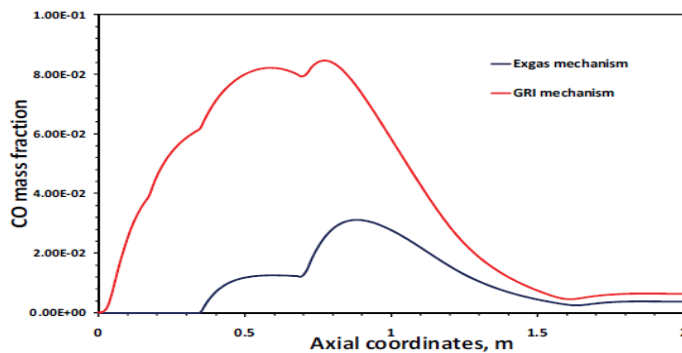


Figure 8: Comparison of the CFD predicted CO at the center line.

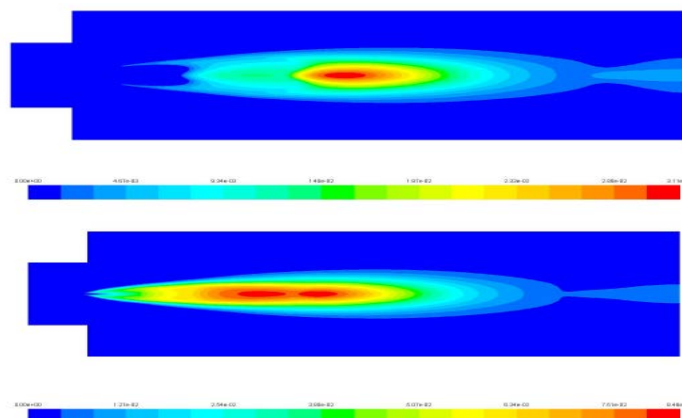


Figure 9: CO contours, EXGAS mechanism (top), GRI mechanism (bottom)

The predicted mass fraction of CO along the centreline is very different, not only that the predictions from the

GRI mechanism are much higher than those from the EXGAS mechanism, almost four times higher in certain regions, but also the profile shape is not quite the same. Furthermore the predicted peaks of mass fractions of CO peak are located in different positions in the flame region and the peak value obtained from the GRI mechanism is around 0.0084 while it is only about 0.0032 from the EXGAS mechanism. This difference is likely due to the fact that the EXGAS model includes more reactions and species (448, 100) than the GRI mechanism (279, 49). More work should be focused in the future on investigating this discrepancy for which a proper validation data set will be required.

8. Conclusion

Numerical study of reacting flow in a three-dimensional methane burner has been carried out using the RANS equations approach. The SST model and the steady flamelet combustion model with detailed reaction mechanism have been used to simulate the fully turbulent reactive flow field in the burner. The effect of the radiation/turbulence interactions have been considered in this paper. The spherical harmonic P-1 method, the gray medium assumption and the Planck-mean absorption coefficients were used to determine the radiative properties of the gas-phase species as a function of temperature. The accuracy of a detailed chemical reaction mechanism for the methane oxidation developed using EXGAS computer package has been assessed by comparing the results from the established GRI mechanism and the limited available experimental data.

The predicted temperature profiles at the flow exit from both mechanisms are very similar and follow the experimental data reasonably well too. With careful strategy of modeling, the simulations using the RANS approach are capable of successfully predicting the temperature field. The structure of the flame computed by the flamelet model using EXGAS mechanism is in agreement with that from the GRI mechanism. The predicted peak concentrations of CO₂ and H₂O from both mechanisms agree with each other very well and the peak locations are the same too. However, there are substantial differences between the two mechanisms for the CO prediction and further study is needed in this area. This paper demonstrates that the EXGAS chemical reaction mechanism for the methane oxidation is capable of adequately predicting the flame temperature as well as the concentrations of the major combustion products.

References

- [1] Peters. N. (1986) Laminar flamelet concepts in turbulent combustion, Twenty first Symposium (International) on Combustion, The Combustion Institute, Pittsburgh, pp. 1231-1250.
- [2] Poinsot, T. and Veynante, D. Theoretical and numerical combustion. RT Edwards, Inc. 2005.
- [3] Champion, M. and Libby, P.A. (1984) Turbulent premixed combustion in a boundary layer. Combustion Science and Technology, volume 38. number 5. pp. 267-291.
- [4] Launder, B.E and Spalding. D.B, (1974) The numerical computation of turbulent flows, Comput. Meths. Appl. Mech. Eng. 3, pp. 269-289.

- [5] Liew. S.K, Bray. K.N.C, Moss. J.B, (1981) Flamelet model of turbulent non-premixed combustion, *Combust. Sci. Technol.* 27 . pp. 69-73.
- [6] Balthasar. M, Heyl. H, Mau. F, Schmitt. F, Bockhorn. H. (1996) Flamelet modeling of soot formation in laminar ethyne/air diffusion flames. *Proc. Combust. Inst.* 26 . pp. 2369-2377.
- [7] Pitsch, H., Barths, H., Peters, N., 1996. Three-dimensional modeling of NO_x and soot formation in DI-diesel engines using detailed chemistry based on the interactive flamelet approach, SAE-paper 962057.
- [8] Mauss, F., Balthasar, M., Simplification of a detailed kinetic soot model for the application in 3D-programs. In: Fourth International Conference on Technologies and Combustion for a Clean Environment, Lissabon, (1997). pp. 17.
- [9] Lentini, D., Puri, I., (1995) Stretched laminar flamelet modeling of turbulent chloromethane-air nonpremixed jet Pames. *Combust. Flame* 103 . pp. 328.
- [10] Pfuderer, D.G., Neuber, A.A., Fruchtel, G., Hassel, E.P., Janicka, J. (1996) Turbulence modulation in jet diffusion flames: modeling and experiments. *Combust. Flame* 106, pp. 301.
- [11] Vranos, A., Knight, B.A., Proscia, W.M., Chiappetta, L., Smooke, M.D., (1992) Nitric oxide formation and differential diffusion in a turbulent methane-hydrogen diffusion flame. In: 24th Symposium (International) on Combustion, The Combustion Institute, Pittsburgh, pp. 377.
- [12] Sanders, J.P.H., Chen, J.-Y., Gokalp, I. (1997) Flamelet-based modeling of NO formation in turbulent hydrogen jet diffusion flames. *Combust. Flame.* 111, pp. 1-15.
- [13] Bowman, C.T., Hanson, R.K., Davidson, D.F., Gardiner, W.C. Jr., Lissianski, V., Smith, G.P., Golden, D.M., Frenklach, M., Wang, H., Goldenberg, M., 1995. GRI-Mech Version 2.11, <http://www.gri.org/>.
- [14] Warth, V., Stef. N., Glaude, P.A., Battin-Leclerc, F., Scacchi, G., Cme. G.M., (1998). Computer based generation of reaction mechanisms for gas-phase oxidation. *Combust. Flame* 114, pp. 81-102.
- [15] Buda. F., Bounaceur. R., Warth. V., Glaude. P.A., Fournet. R., Battin-Leclerc. F., (2005) Progress toward a unified detailed kinetic model for the autoignition of alkanes from C₄ to C₁₀ between 600 and 1200 K. *Combust. Flame*, 142, pp. 170-186.
- [16] Biet. J., Hakka M.H., Warth. V., Glaude. P.A., Battin-Leclerc. F. (2008) Experimental and Modeling Study of the Low-Temperature Oxidation of Large Alkanes. *Energy and Fuel*, 22 pp. 2258-2269.
- [17] Glaude. P.A., Battin-Leclerc. F., Fournet. R., Warth. V., Cme. G.M., Scacchi. G. (2000) Construction and simplification of a model for the oxidation of alkanes. *Combust. Flame* 122, pp. 451-462.
- [18] Touchard. S., Fournet. R., Glaude. P.A., Warth. V., Battin-Leclerc. F., Vanhove. G., Ribaucour. M.,

- Minetti. R., (2005) Proc. Combust. Inst. 30, pp. 1073-1081.
- [19] Modest, M.F, Radiative heat transfer, Academic Press, 2003.
- [20] Barlow, R. S., Chen, J.-Y., Smith, N. S. A. and Bilger, R. W. (1999), Combust. Flame 117, pp. 4-31.
- [21] Grosshandler, W.L. (1993) RADCAL: A narrow-band model for radiation calculations in a combustion
- [22] Ilbasa, M., Ylmaza, I., Kaplan, Y., (2005) Investigations of hydrogen and hydrogenhydro-carbon composite fuel combustion and NO_x emission characteristics in a model combustor. International Journal of Hydrogen Energy 30, pp.1139-1147. environment. NIST Technical Note 1402 (April).
- [23] Chen, J.Y., (1998) Experimental and numerical study of a highly diluted turbulent diffusion flame close to blow-out. In: 27th Symposium (International) on Combustion, The Combustion Institute, Pittsburgh, pp. 307.
- [24] Chou, C.-P., Chen, J.-Y., Yam, C.G., Marx, K., (1998) Numerical modeling of NO_x formation in laminar bunsen flames- a flamelet approach. Combust. Flame 114, pp. 420-435.
- [25] Battin-LeClerc. F, Bounaceur. R, Cme. G.M, (2004) EXGAS-ALKANES, a software for the automatic generation of mechanisms for the oxidation of alkanes, CNRS-DCPR.
- [26] Williams, F.A. Combustion theory. Perseus Books, 1985.
- [27] Borghi, R. and Champion, M. Modelisation et theorie des flammes. Editions Technip. 2000.
- [28] Menter, F.R., (1993) Zonal two Equation k- ϵ Turbulence Models for Aerodynamic Flows, AIAA 93-2906.
- [29] Cant, R.S., Rogg, B., Bray, K.N.C., (1989) Flamelet modelling in premixed turbulent combustion, Proceeding of the Joint Meeting of the British and French Sections of the Combustion Institute, Rouen, France, pp. 191-196.
- [30] Liew, S.K., Bray, K.N.C., Moss, J.B. (1984) A stretched laminar flamelet model of turbulent nonpremixed combustion. Combust. Flame 56, 1984.